Supplemental Document

Optics Letters

Perturbation approach to improve the angular tolerance of high-Q resonances in metasurfaces: supplement

Guilherme S. Arruda,[1,*] Donato Conteduca,[2] Isabel Barth,[2] Yue Wang,[2] Thomas F. Krauss,[2] and Emiliano R. Martins[1]

[1] *São Carlos School of Engineering, Department of Electrical and Computer Engineering, University of São Paulo, São Carlos-SP, Brazil*
[2] *Photonics Group, School of Physics, Engineering and Technology, University of York, Heslington, York YO10 5DD, UK*
[*] *Corresponding author: guilherme.simoneti.arruda@usp.br*

Supplement DOI: https://doi.org/10.6084/m9.figshare.21424329

Parent Article DOI: https://doi.org/10.1364/OL.475601

Perturbation approach to improve the angular tolerance of high-Q resonances in metasurfaces: supplemental document

1. DERIVATION OF EQUATION 3 OF THE MAIN TEXT

We begin with equation 1 of the main text:

$$A(\omega, k) \approx \left| \frac{Q_R^{-1}}{2i\left(1 - \frac{\omega}{\omega_0(k)}\right) + Q_R^{-1} + Q_{NR}^{-1}} \right|^2 \tag{S1}$$

This equation expresses the resonance amplitude as a function of frequency ω and momentum k. In a typical band dispersion diagram, k is the wavevector component parallel to the metasurface plane. The dependence on k enters through the resonance frequency $\omega_0(k)$, which is a function of k. As discussed in the main text, the dispersion band around the Γ point of the Brillouin zone in photonic resonators is typically parabolic, so the resonance frequency dependence on the parallel component k can be approximated by a quadratic form:

$$\omega_0(k) = \omega_0 \pm \alpha k^2 \tag{S2}$$

Where α represents the curvature of the mode's band diagram and ω_0 is the resonance frequency at the Γ point ($k = 0$). A convenient way of quantifying the angular tolerance is to inspect the behaviour of the resonance amplitude at a fixed frequency as k is changed. Therefore, to quantify the angular tolerance, we can find the range of values of k for which the amplitude at ω_0 varies within a tolerance range. Thus, defining the tolerance range as the Full Width of Half Maximum (FWHM) value [1–3], we impose that:

$$A(\omega_0, \Delta k) = \frac{A(\omega_0, 0)}{2} \tag{S3}$$

where Δk is the FWHM angular tolerance of the structure. The physical meaning of Δk is illustrated in Fig. S1:

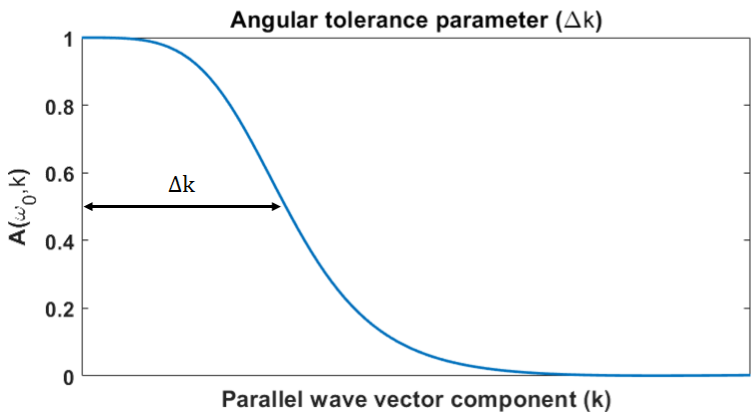

Fig. S1. Illustration of the physical meaning of the angular tolerance Δk. The angular tolerance is the range within which the amplitude of the resonance is higher than half of its peak value.

Substituting equation S2 into equation S1, we find:

$$A(\omega,k)=\left|\frac{Q_R^{-1}}{2i\left(1-\frac{\omega}{\omega_0\pm\alpha k^2}\right)+Q_R^{-1}+Q_{NR}^{-1}}\right|^2 \tag{S4}$$

where we dropped the approximation sign to clean up the notation. From equation S4 we readily infer that:

$$A(\omega_0,0)=\left|\frac{Q_R^{-1}}{2i\left(1-\frac{\omega_0}{\omega_0}\right)+Q_R^{-1}+Q_{NR}^{-1}}\right|^2=\left|\frac{Q_R^{-1}}{Q_R^{-1}+Q_{NR}^{-1}}\right|^2=\frac{1}{\left(1+\frac{Q_R}{Q_{NR}}\right)^2} \tag{S5}$$

and

$$A(\omega_0,\Delta k)=\left|\frac{Q_R^{-1}}{2i\left(1-\frac{\omega_0}{\omega_0\pm\alpha(\Delta k)^2}\right)+Q_R^{-1}+Q_{NR}^{-1}}\right|^2=\left|\frac{1}{2Q_R\left(1-\frac{\omega_0}{\omega_0\pm\alpha(\Delta k)^2}\right)i+1+\frac{Q_R}{Q_{NR}}}\right|^2$$
$$=\frac{1}{4Q_R^2\left(1-\frac{\omega_0}{\omega_0\pm\alpha(\Delta k)^2}\right)^2+\left(1+\frac{Q_R}{Q_{NR}}\right)^2} \tag{S6}$$

Substituting equations S5 and S6 into equation S3, we obtain:

$$\frac{1}{4Q_R^2\left(1-\frac{\omega_0}{\omega_0\pm\alpha(\Delta k)^2}\right)^2+\left(1+\frac{Q_R}{Q_{NR}}\right)^2}=\frac{1}{2\left(1+\frac{Q_R}{Q_{NR}}\right)^2} \tag{S7}$$

from which we readily infer that:

$$4Q_R^2\left(1-\frac{\omega_0}{\omega_0\pm\alpha(\Delta k)^2}\right)^2=\left(1+\frac{Q_R}{Q_{NR}}\right)^2 \tag{S8}$$

and with the help of equation S5, equation S8 can be recast as:

$$1-\frac{\omega_0}{\omega_0\pm\alpha(\Delta k)^2}=\frac{1}{2Q_R\sqrt{A(\omega_0,0)}} \tag{S9}$$

then, rearranging equation S9, we obtain:

$$(\Delta k)^2=\frac{\omega_0}{\alpha}\frac{1}{2Q_R\sqrt{A(\omega_0,0)}-1} \tag{S10}$$

Typically, specially for high-Q resonances, we have $2Q_R\sqrt{A(\omega_0,0)}>>1$, allowing the following approximation:

$$(\Delta k)^2=\frac{\omega_0}{\alpha}\frac{1}{2Q_R\sqrt{A(\omega_0,0)}} \tag{S11}$$

thus, finally, we obtain:

$$\Delta k=\sqrt{\frac{\omega_0}{2\alpha Q_R}}\left(\frac{1}{A(\omega_0,0)}\right)^{1/4} \tag{S12}$$

which is the equation 3 of the main text.

2. DERIVATION OF EQUATION 5 OF THE MAIN TEXT

Extending equation 4 of the main text to a square lattice with four structures, as shown in figure 1c of the main text, we obtain:

$$c_{mn} = a_{mn}\left[e^{-i\left(\frac{2\pi m}{\Lambda}x_1+\frac{2\pi n}{\Lambda}y_1\right)} + e^{-i\left(\frac{2\pi m}{\Lambda}x_2+\frac{2\pi n}{\Lambda}y_2\right)} + e^{-i\left(\frac{2\pi m}{\Lambda}x_3+\frac{2\pi n}{\Lambda}y_3\right)} + e^{-i\left(\frac{2\pi m}{\Lambda}x_4+\frac{2\pi n}{\Lambda}y_4\right)}\right] \quad \text{(S13)}$$

where $\overrightarrow{r}_p = x_p\hat{x} + y_p\hat{y}$, with $p = 1,2,3,4$ are the position vectors and a_{mn} are the Fourier components of the un-perturbed nano-hole array (deduced further in the text). For a symmetric shift, we have $\overrightarrow{r}_1 = -\overrightarrow{r}_3$ and $\overrightarrow{r}_2 = -\overrightarrow{r}_4$. Consequently, equation S13 reduces to:

$$c_{mn} = 2a_{mn}\left[cos\left(\frac{2\pi m}{\Lambda}x_1 + \frac{2\pi n}{\Lambda}y_1\right) + cos\left(\frac{2\pi m}{\Lambda}x_2 + \frac{2\pi n}{\Lambda}y_2\right)\right] \quad \text{(S14)}$$

Defining the reference position vectors as:

$$\begin{aligned}
\overrightarrow{r}_{10} &= \frac{\Lambda}{4}\hat{x} + \frac{\Lambda}{4}\hat{y}\\
\overrightarrow{r}_{20} &= -\frac{\Lambda}{4}\hat{x} + \frac{\Lambda}{4}\hat{y}\\
\overrightarrow{r}_{30} &= -\overrightarrow{r}_{10}\\
\overrightarrow{r}_{40} &= -\overrightarrow{r}_{20}
\end{aligned} \quad \text{(S15)}$$

and the perturbation vectors as:

$$\begin{aligned}
\overrightarrow{r}_{1\delta} &= \delta\hat{x} + \delta\hat{y}\\
\overrightarrow{r}_{2\delta} &= -\delta\hat{x} + \delta\hat{y}\\
\overrightarrow{r}_{3\delta} &= -\overrightarrow{r}_{1\delta}\\
\overrightarrow{r}_{4\delta} &= -\overrightarrow{r}_{2\delta}
\end{aligned} \quad \text{(S16)}$$

we can express the position vector as $\overrightarrow{r}_p = \overrightarrow{r}_{p0} + \overrightarrow{r}_{p\delta}$, which entails that $x_1 = y_1 = \Lambda/4 + \delta$ and $x_2 = -y_2 = -(\Lambda/4 + \delta)$. With these identities, equation S14 reduces to:

$$c_{mn} = 2a_{mn}\left\{cos\left[\left(\frac{2\pi m}{\Lambda} + \frac{2\pi n}{\Lambda}\right)\left(\frac{\Lambda}{4} + \delta\right)\right] + cos\left[\left(-\frac{2\pi m}{\Lambda} + \frac{2\pi n}{\Lambda}\right)\left(\frac{\Lambda}{4} + \delta\right)\right]\right\} \quad \text{(S17)}$$

following that:

$$c_{0n} = c_{n0} = 4a_{n0}cos\left[\left(\frac{2\pi}{\Lambda}n\right)\left(\frac{\Lambda}{4} + \delta\right)\right] \quad \text{(S18)}$$

which is equation 5 of the main text. The dependence of the function $cos\left[\left(\frac{2\pi}{\Lambda}n\right)\left(\frac{\Lambda}{4} + \delta\right)\right]$ on δ is shown in Fig. S2.

Now, the Fourier components of the unperturbed nano-hole array are given by:

$$\begin{aligned}
a_{mn} &= 2(\epsilon_l - \epsilon_h)FF\frac{J_1\left(\frac{\pi}{\Lambda}\sqrt{m^2+n^2}W\right)}{\frac{\pi}{\Lambda}\sqrt{m^2+n^2}W}\ ; m,n \neq 0\\
a_{00} &= FF\epsilon_l + (1-FF)\epsilon_h
\end{aligned} \quad \text{(S19)}$$

Where ϵ_l and ϵ_h are respectively the dielectric constants of the hole and slab, J_1 is the Besssel function of first order, W is the hole diameter and FF is the fill factor:

$$FF = \frac{\pi\left(\frac{W}{2}\right)^2}{\Lambda^2} \quad \text{(S20)}$$

Thus, the first and second Fourier components of the PNHA are given by equation 5 of the main text, with a_{mn} given by equation S19.

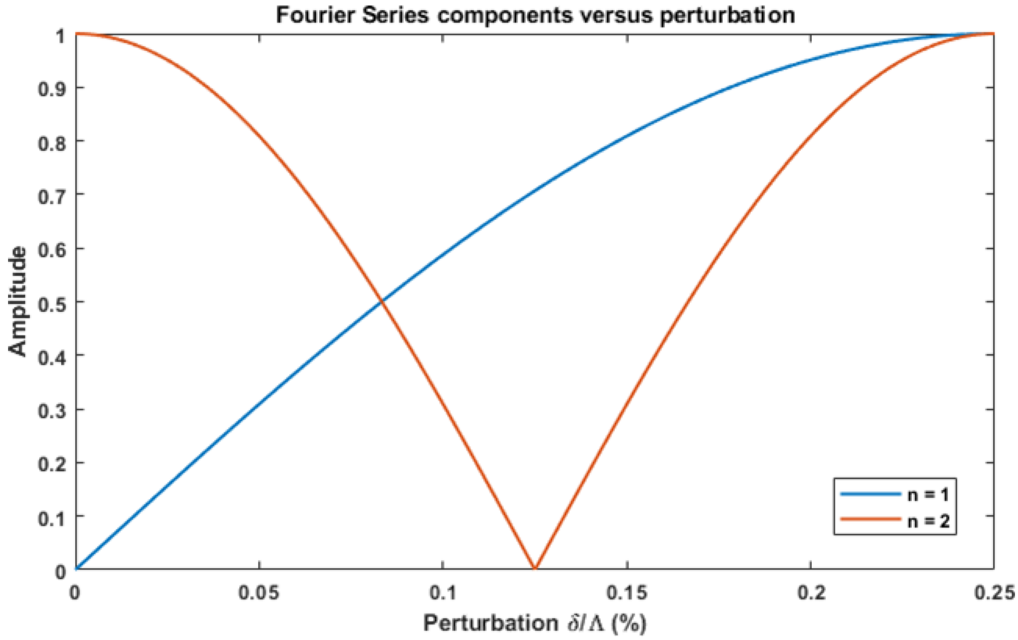

Fig. S2. The dependence of the function $cos\left[\left(\frac{2\pi}{\Lambda}n\right)\left(\frac{\Lambda}{4}+\delta\right)\right]$ on the perturbation parameter δ.

3. BAND DIAGRAM OF THE METASURFACE WITH ELLIPTICAL META-ATOMS

Here we show that the metasurface with elliptical meta-atoms proposed in [4] shares the properties of both the perturbed nano hole array (PNHA) metasurface and also the symmetry protected BIC. When the ellipses are tilted, as shown in Fig. S3a, the new period Λ_x is twice as large as the unperturbed period, and can excite a mode with propagation constant β_x:

$$\frac{2\pi}{\Lambda_x} = \beta_x \tag{S21}$$

However, when $\phi = 0$, the period becomes halved and, clearly, the structure no longer couples the same mode as before, just like the perturbated metasurface. Thus, the unperturbed structure (as shown under the label "not tilted" in Fig. S3b) features a bound mode, but this mode is not in the continuum, and so it is not a BIC.

The perturbed structure, however, does feature a symmetry protected BIC. The BIC nature of the perturbed structure can be better visualised if the perturbation is such that the period is doubled, but the symmetry is not broken. This perturbation can be achieved by shifting the ellipses towards each other, thus creating a new unit cell with period Λ_x, as shown in Fig. S3c. The band structure (Fig. S3d) vanishes at the Γ ($k = 0$) point, which is the signature of a symmetry protected BIC. The tilting of the ellipses angle (ϕ) breaks the symmetry of the geometry, thus the modes radiates, with the Q-factor proportional to ϕ, as seen in Fig. S3e.

As such, the metasurface with elliptical meta-atoms is intermediary between BIC and PNHA, featuring properties of both types of structures. This effect manifest itself on the angular tolerance of these structures: it is higher than the regular BIC angular tolerance, while being lower than that of the PHNA, as illustrated in Fig. S4a. It also shows the same property of decreasing α with increasing Q-factor (Fig. S4b), like the PHNA (Fig. S4c) and in contrast to the NHA (Fig. S4d). However, the α values for the metasurface with elliptical meta-atoms are not so low as the ones for the PHNA, which translates to a worse angular tolerance performance. The geometry used for the metasurface with elliptical meta-atoms is the same as in Fig. S4e, while the geometries used for both the PHNA and NHA are the same used in Fig. 4 of the main paper.

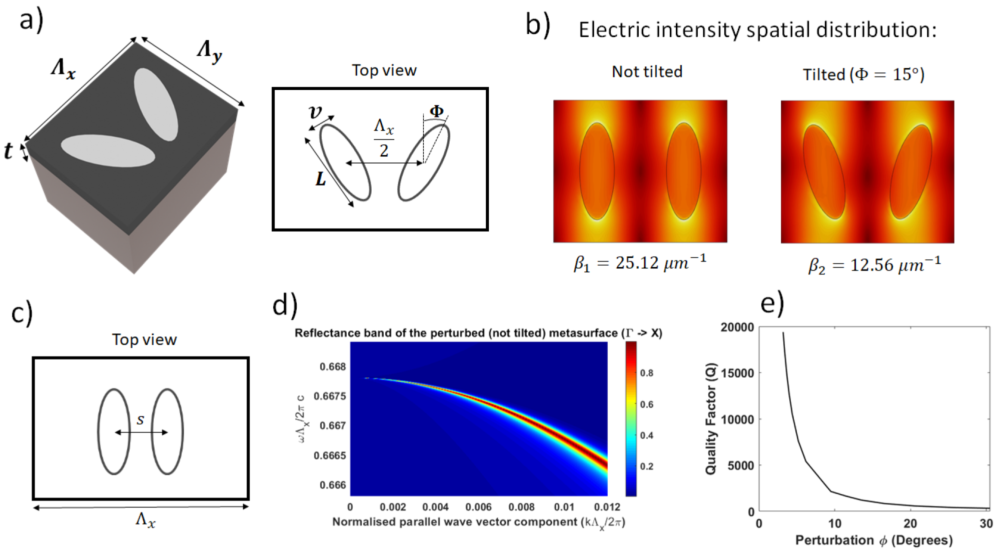

Fig. S3. a) Metasurface with elliptical meta-atoms. The cover is assumed to be water ($n = 1.33$), the substrate (light brown) to be glass ($n = 1.45$) and the core (dark grey) has a refractive index of $n = 2.4$. The geometrical parameters of the elliptical metasurface are: $\Lambda_y = 0.82\Lambda_x$, $t = 0.36\Lambda_x$, $L = 0.56\Lambda_x$ and $v = 0.2\Lambda_x$. b) Electric field distribution of the un-perturbed (not tilted) and perturbed (tilted) elliptical metasurfaces for the specific case where $\Lambda_x = 500$nm. When the tilting angle $\Phi = 0$, the period of the structure is halved and the mode's propagation constant β_1 is equal to 25.12 μm^{-1}, note that this value is equal to $2\pi/(\Lambda_x/2)$. Thus, whereas this is a bound mode, it is not in the continuum. If $\Phi \neq 0$ and/or the distance between the centre of the ellipsis is perturbed, the mode changes to $\beta_2 = 12.56\ \mu m^{-1}$, which is precisely half β_1 and equal to $2\pi/\Lambda_x$. The band diagram of the elliptical metasurface (c) with $\Phi = 0$ and perturbed distance $s < \Lambda_x/2 = 0.32\Lambda_x$ is shown in (d), where, at the Γ point, it exhibits a BIC. The typical dependence of the mode's Q-factor of a metasurface with elliptical meta-atoms on ϕ is also shown (e). Similar to the PHNA, the Q-factor goes to infinity as ϕ approaches zero. In all structures.

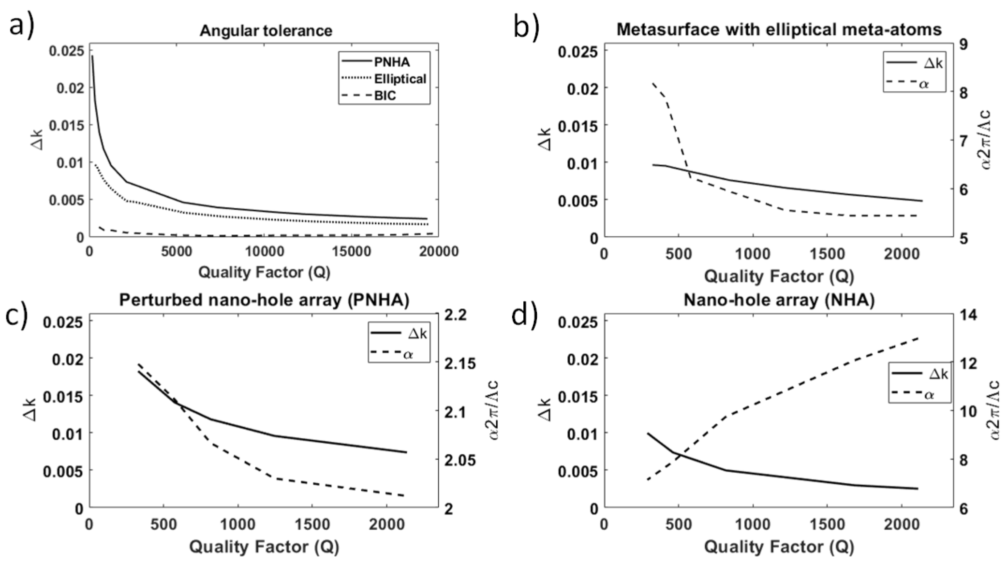

Fig. S4. a) Angular tolerance comparison between the PHNA, BIC and the metasurface with elliptical meta-atoms. The PHNA, NHA and BIC structures are the same as in the main paper (figures 3 and 4), while the metasurface with elliptical meta-atoms is the same as in the figure S3e. The relation between the angular tolerance Δk, α and Q-factor for the three structures is shown in b) (Ellipses), c) (PHNA) and d) (BIC/NHA).

4. MORE EXAMPLES OF DEPENDENCE OF THE Q-FACTOR AND α ON δ

Here we shown the perturbation method applied to periodic structures of different materials than that of the main text. The first structure consists of a nano-hole array (NHA) carved into a high dielectric film immersed in air, as depicted in Fig. S5a and S5b, respectively in both their perturbed (high-n-PNHA) and non-perturbed (high-n-NHA) configurations. The other structure (Fig. S5c and S5d) consists of nano holes carved into a thin metal film over a hybrid substrate. The metallic-NHA (Fig. S5d) was designed based on the structure investigated in [5]. Details of the refractive indexes used in the simulations are given in the legend of Fig. S5.

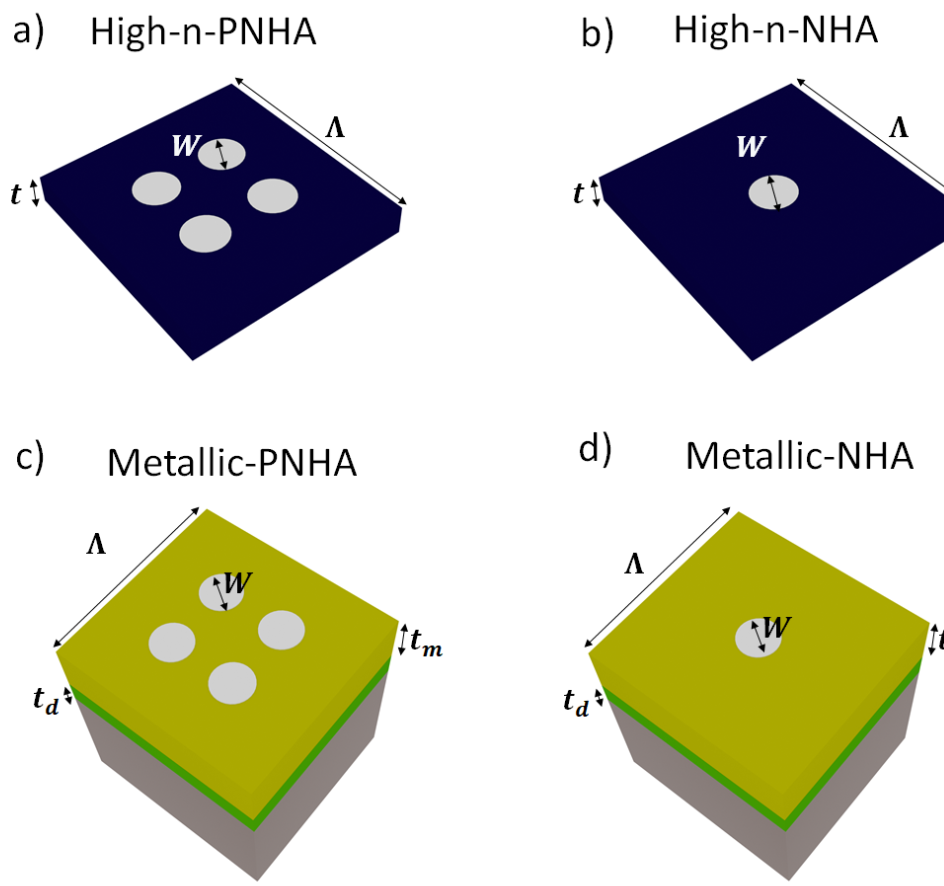

Fig. S5. Unit cell of the high-n-PNHA, consisting of a set of four nano-holes of diameter W etched into a thin film of a high dielectric material (dark blue, $n = 3.5$) with thickness t. b) nano-hole array (NHA) etched into a thin film of a high dielectric material (dark blue, $n = 3.5$) with thickness t. The structures are surrounded by air (white background). c) Unit cell of the metallic-PHNA, consisting of a set of four nano-holes of diameter W etched into a thin gold (Au) film of thickness t_m over a hybrid substrate composed of a thin dielectric layer (green, $n = 2$) of thickness t_d and a slab of glass (light brown, $n = 1.45$). d) metallic-NHA etched on the same film and substrate of c).

The relation between the band's curvature α, the mode's Q-factor and its angular tolerance (Δk) is shown in Fig. S6 for both high-n (Figs. S6a and S6b) and metallic structures (Figs. S6c and S6d).

It is clear that, in agreement with the results shown in the main paper, the perturbed structures exhibited decreasing α for higher Q-factors (Figs. S6a and S6c), in contrast to the unperturbed versions (Figs. S6b and S6d), where α increases with the Q-factor. Since both α and the Q-factor contribute equally to the angular tolerance, the reduction of α for higher Q-factors in the perturbed structures leads to better angular tolerances.

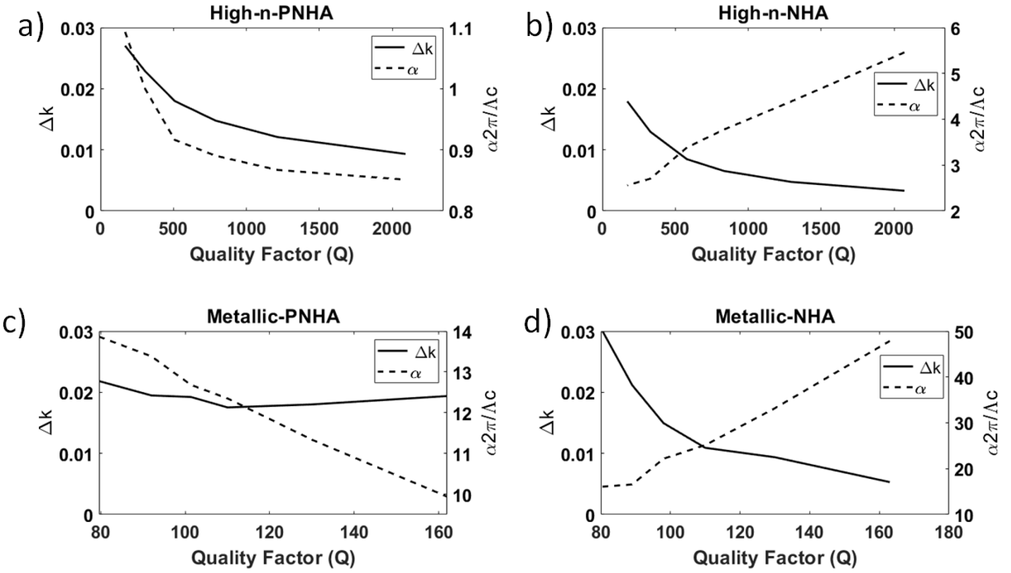

Fig. S6. Angular tolerance (Δk) and band's curvature (α) of the high-n-PNHA (a), high-n-NHA (b), metallic-PNHA (c) and metallic-NHA (d). The geometrical parameters of high-n-PHNA (a) are: $t = 0.42\Lambda$,$W = 0.28\Lambda$, and δ/Λ varying from 1.33% (highest Q-factor) up to 4.28% (lowest Q-factor). The period of the high-n-NHA was slightly adjusted to keep the resonance wavelength fixed, with parameters being, for a starting period Λ_0 (highest Q-factor), as follows (b): $\Lambda = \lambda_0 \rightarrow 1.107\Lambda_0$, t= $0.43\lambda_0$, $W = 0.19\Lambda_0 \rightarrow 0.43\Lambda_0$ (highest to lowest Q-factor). The geometrical parameters of the metallic-PHNA (c) are: $t_m = 0.16\Lambda$,$t_d = 0.09\Lambda$,$W = 0.27\Lambda$, and δ/Λ varying from 6.07% (highest Q-factor) up to 8.6% (lowest Q-factor). The geometrical parameters of metallic-HNA (d) are $t_m = 0.16\Lambda$,$t_d = 0.09\Lambda$, $W = 0.18\Lambda \rightarrow 0.33\Lambda$ (highest to lowest Q-factor. The Q-factor of the unperturbed metasurfaces were varied by controlling the hole's diameter.

5. BAND CURVATURES OF THE PNHA STRUCTURES

In Fig. S7 we illustrate the impact of the perturbation parameter δ on the mode's band curvature α and Q-factor of the PNHA structures (Fig. S7a), with the same materials as the high-n-PNHA of Fig. S5a, for different δ values (Figs. S7b to S7c), where it can be seen that, as the perturbation δ decreases, the Q-factor increases, which is evident by the tuning of the mode's band, and the band's curvature also decreases, flattening the band.

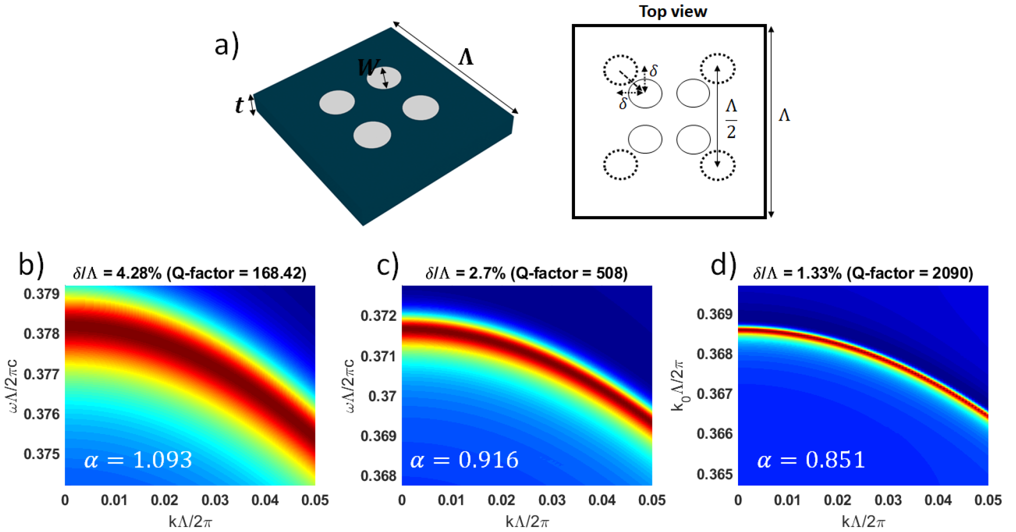

Fig. S7. a) Perturbed nano-hole array (PNHA) and the perturbation parameter δ. The materials used in the simulation are identical of those used in figure S5b. The geometrical parameters of high-n-PHNA (a) are: $t = 0.42\Lambda$, $W = 0.28\Lambda$. The band curvature α is given in normalised units of $\alpha 2\pi/\Lambda c$.

REFERENCES

1. F. Lemarchand, A. Sentenac, and H. Giovannini, "Increasing the angular tolerance of resonant grating filters with doubly periodic structures," Opt. letters **23**, 1149–1151 (1998).
2. F. Lemarchand, A. Sentenac, E. Cambril, and H. Giovannini, "Study of the resonant behaviour of waveguide gratings: increasing the angular tolerance of guided-mode filters," J. Opt. A: Pure Appl. Opt. **1**, 545 (1999).
3. A. Mizutani, H. Kikuta, and K. Iwata, "Wave localization of doubly periodic guided-mode resonant grating filters," Opt. review **10**, 13–18 (2003).
4. F. Yesilkoy, E. R. Arvelo, Y. Jahani, M. Liu, A. Tittl, V. Cevher, Y. Kivshar, and H. Altug, "Ultrasensitive hyperspectral imaging and biodetection enabled by dielectric metasurfaces," Nat. Photonics **13**, 390–396 (2019).
5. A. E. Cetin, D. Etezadi, B. C. Galarreta, M. P. Busson, Y. Eksioglu, and H. Altug, "Plasmonic nanohole arrays on a robust hybrid substrate for highly sensitive label-free biosensing," ACS photonics **2**, 1167–1174 (2015).